



## Retention of $^{99m}\text{Tc}$ at Ultra-trace Levels in Flowing Column Experiments – Insights into Bioreduction and Biomineralization for Remediation at Nuclear Facilities

Clare L. Thorpe, Jonathan R. Lloyd, Gareth T. W. Law, Heather A. Williams, Nick Atherton, Julian H. Cruickshank & Katherine Morris

To cite this article: Clare L. Thorpe, Jonathan R. Lloyd, Gareth T. W. Law, Heather A. Williams, Nick Atherton, Julian H. Cruickshank & Katherine Morris (2016) Retention of  $^{99m}\text{Tc}$  at Ultra-trace Levels in Flowing Column Experiments – Insights into Bioreduction and Biomineralization for Remediation at Nuclear Facilities, *Geomicrobiology Journal*, 33:3-4, 199-205, DOI: [10.1080/01490451.2015.1067656](https://doi.org/10.1080/01490451.2015.1067656)

To link to this article: <https://doi.org/10.1080/01490451.2015.1067656>



© 2016 Taylor & Francis Group, LLC



Published online: 25 Feb 2016.



[Submit your article to this journal](#)



Article views: 665



[View related articles](#)



[View Crossmark data](#)



Citing articles: 9 [View citing articles](#)

## Retention of $^{99m}\text{Tc}$ at Ultra-trace Levels in Flowing Column Experiments – Insights into Bioreduction and Biomineralization for Remediation at Nuclear Facilities

Clare L. Thorpe<sup>a</sup>, Jonathan R. Lloyd<sup>a</sup>, Gareth T. W. Law<sup>b</sup>, Heather A. Williams<sup>c</sup>, Nick Atherton<sup>d</sup>, Julian H. Cruickshank<sup>d</sup>, and Katherine Morris<sup>a</sup>

<sup>a</sup>Research Centre for Radwaste Disposal and Williamson Research Centre for Molecular Environmental Science, School of Earth, Atmospheric and Environmental Sciences, The University of Manchester, Manchester, United Kingdom; <sup>b</sup>Centre for Radiochemistry Research, School of Chemistry, The University of Manchester, Manchester, United Kingdom; <sup>c</sup>Nuclear Medicine Centre, Manchester Royal Infirmary, Manchester, United Kingdom; <sup>d</sup>Sellafield Ltd., Land Quality, Sellafield, Seascale, Cumbria, United Kingdom

### ABSTRACT

The behavior of technetium at ultra-trace ( $<10^{-10}$  mol  $\text{l}^{-1}$ ) concentrations in bioreducing sediment column experiments was investigated using  $^{99m}\text{Tc}$   $\gamma$ -camera imaging. Four flowing sediment columns were biostimulated for varying periods of time, using acetate as an electron donor, such that on the day of imaging they represented oxic, early metal-reducing, Fe(III)-reducing and sulfate-reducing conditions. Prior to imaging, columns were spiked with 9.6 MBq of  $^{99m}\text{Tc}(\text{VII})\text{O}_4^-$ , which is relevant to the  $^{99}\text{Tc}$  mass concentrations observed at nuclear facilities, run under site relevant flow conditions, and imaged using  $\gamma$ -camera imaging at 20 min intervals over 12h. In the oxic column  $^{99m}\text{Tc}$  behaved as a conservative tracer and did not interact significantly with the sediment. In all of the biostimulated columns  $^{99m}\text{Tc}$  associated with the sediment although the spike was least mobile in the order sulfate < Fe(III)-reducing < early metal-reducing columns, confirming higher reactivity for  $^{99m}\text{Tc}$  under increasingly reducing conditions. Columns were destructively sampled after  $^{99m}\text{Tc}$  decay (5 days storage), and 0.5 N HCl extractable Fe as Fe (II) was measured at 2 cm intervals along the column length. The Fe(II) measured in all electron donor amended columns was present in stoichiometric excess to the  $^{99m}\text{Tc}$ . Geochemical modelling and aqueous geochemical data from the different biostimulation treatments suggested that the elevated pH observed in the more reduced columns lead to increased sorbed and mineral associated Fe(II), both stronger reductants for Tc(VII) than aqueous Fe(II). In the sulfate reduction column the presence of FeS lead to the fastest rates of  $^{99m}\text{Tc}$  immobilization. The results are the first to show the variable but significant retention of  $^{99m}\text{Tc}$  at ultra-trace levels relevant to conditions at many nuclear sites in a range of biostimulated sediment columns and present a positive outlook for the treatment of  $^{99}\text{Tc}$  contaminated groundwater through in-situ biostimulation.

### ARTICLE HISTORY

Received May 2015  
Accepted May 2015

### KEYWORDS

Biomineralization;  
bioremediation; metal  
reduction; sediments



### Introduction

Technetium-99 contaminated groundwater is present at many nuclear sites including the Sellafield nuclear facility, UK (Beals and Hayes 1995; Serne and Rapko 2014; Stamper et al. 2014). Due to its long half-life ( $2.1 \times 10^5$  years)  $^{99}\text{Tc}$  is a key risk-driving radionuclide in many safety case scenarios and the behavior of  $^{99}\text{Tc}$  in subsurface environments is of interest from both a radioactively contaminated land and radioactive waste management perspective. At the Sellafield nuclear facility historical releases of radionuclides to groundwater have resulted in an immediate and ongoing need to understand  $^{99}\text{Tc}$  transport in the subsurface and, if possible, investigate techniques that can be used to retard the spread of contaminant plumes.

Stimulation of the subsurface to promote metal reduction has been proposed for the treatment of  $^{99}\text{Tc}$  contaminated groundwater, and soluble Tc(VII) has been shown to be immobilised as poorly soluble Tc(IV) under Fe(III)-reducing conditions (Icenhower et al. 2010; Lloyd et al. 2000; Newsome et al.

2014; Prakash et al. 2013). During bioreduction, the addition of an electron donor, for example acetate, promotes microbial respiration and a cascade of terminal electron accepting process develop as the bacteria couple the oxidation of the electron donor to the reduction of available electron acceptors in the subsurface in the order oxygen > nitrate > manganese > iron > sulfate > methane. The behavior of  $^{99}\text{Tc}$  during bioreduction has been well studied in sediment microcosms (Burke et al. 2010; Eagling et al. 2012; Fredrickson et al. 2004; Law et al. 2010), microbial cultures (Liu et al. 2002; Lloyd et al. 2000) and pure biomineral systems (McBeth et al. 2011; Morris et al. 2008; Peretyazhko et al. 2012; Thorpe et al. 2014).

Although reduction of Tc(VII) to Tc(VI) can occur enzymatically via the hydrogenase enzyme in some metal-reducing bacteria (Lloyd et al. 2000; Marshall et al. 2008) it is generally accepted that, in typical environmental systems, abiotic reduction by Fe(II)-bearing minerals and sorbed Fe(II) dominates (Lloyd et al. 2000; Plymale et al. 2011). The rate of Tc(VII)

**CONTACT** Katherine Morris  Email: [katherine.morris@manchester.ac.uk](mailto:katherine.morris@manchester.ac.uk)  Research Centre for Radwaste Disposal and Williamson Research Centre for Molecular Environmental Science, School of Earth, Atmospheric and Environmental Sciences, The University of Manchester, Manchester, M13 9PL, United Kingdom.  
Color versions for one or more of the figures in the article can be found online at [www.tandfonline.com/ugmb](http://www.tandfonline.com/ugmb).

© 2016 Clare L. Thorpe, Jonathan R. Lloyd, Gareth T. W. Law, Heather A. Williams, Nick Atherton, Julian H. Cruickshank, and Katherine Morris.  
Published with license by Taylor and Francis

This is an open-access article distributed under the terms of the Creative Commons Attribution License <http://creativecommons.org/licenses/by/3.0/>, which permits unrestricted use, distribution, and reproduction in any medium, provided the original work is properly cited. The moral rights of the named author(s) have been asserted.

reduction by Fe(II) is dependent on Fe(II) speciation with Fe(II) sorbed to Fe(III) oxides and Fe(II)-bearing minerals magnetite, green rust and iron sulfides yielding greater  $^{99}\text{Tc(VII)}$  reduction rates than siderite and vivianite (Bishop et al. 2012; Burke et al. 2010; Fredrickson et al. 2004; Liu et al. 2008; Liu et al. 2012; Livens et al. 2004; Peretyazhko et al. 2012; Pepper et al. 2003) and with aqueous Fe(II) being the least effective  $^{99}\text{Tc(VII)}$  reductant (Lloyd et al. 2000; Zachara et al. 2007).

These studies have identified pH as a key control on the speciation of Fe(II), with higher pH promoting Fe(II)-bearing mineral precipitation and sorption of Fe(II) to mineral surfaces and thus favouring elevated Tc(VII)-reduction rates (Peretyazhko et al. 2012). Although Fe(III)-reduction has been identified as a key biogeochemical process in controlling  $^{99}\text{Tc}$  mobility, sediment studies have reported higher removal rates and partition coefficients (Kd) for  $^{99}\text{Tc}$  in sulfidic sediments when compared to Fe(III)-reducing sediments without sulfides present (Burke et al. 2010; Lee et al. 2014). Pure mineral studies confirmed that amorphous iron sulfide rapidly reduced  $\text{TcO}_4^-$  at circumneutral pH with the reaction rates increasing with lower pH and higher ionic strength (Liu et al. 2008).

In the majority of studies, the concentration of  $^{99}\text{Tc}$  used was typically  $> 10^{-6}$  M in order to allow the use analytical techniques such as liquid scintillation counting and X-ray spectroscopy. The medical radiotracer  $^{99\text{m}}\text{Tc}$  (half-life 6 h), allows high resolution imaging of sediments containing ultra-trace concentrations of  $^{99\text{m}}\text{Tc}$  (typically  $< 5 \times 10^{-10}$  mol l $^{-1}$ ) making it possible to conduct studies at technetium concentrations typical of far field contamination at nuclear sites down gradient of the contaminant plume source (Burke et al. 2010; Corkhill et al. 2013; Lear et al. 2010; Vandehey et al. 2012), and below the theoretical solubility limit of hydrous  $\text{TcO}_2$  ( $\sim 10^{-8}$  mol l $^{-1}$ ; Hess et al. 2004). At these environmentally relevant concentrations of contaminant, bioavailable Fe will be in stoichiometric excess in typical bioreduced sediments and the rate of Tc(VII) reduction, and the mobility of  $^{99}\text{Tc}$  will be controlled by the Fe(II) speciation (Burke et al. 2010; Peretyazhko et al. 2012; Wildung et al. 2004).

Imaging experiments using  $^{99\text{m}}\text{Tc(VII)}$  have been conducted in sediment microcosms under variable geochemical conditions demonstrating that  $^{99\text{m}}\text{Tc}$  is retained on Fe(III)-reducing sediments at ultra-trace concentrations and proposing reduction to Tc(IV) and sorption to biomineral surfaces as the retention mechanism (Burke et al. 2010; Lear et al. 2010; Vandehey et al. 2012). Under flow conditions in oxic column, experiments focussed on radioactive waste disposal demonstrated that  $^{99\text{m}}\text{Tc(VII)}$  sorption was weak and that under oxic conditions  $^{99\text{m}}\text{Tc}$  acted as a conservative tracer (Corkhill et al. 2013).

In contrast, in experiments designed to explore the impact of biogeochemical processes on  $^{99\text{m}}\text{Tc}$  behavior,  $^{99\text{m}}\text{Tc}$  became strongly associated with reduced, Fe(II)-bearing sediments concentrated at the Fe(II)/Fe(III) redox boundary (Lear et al. 2010). Here,  $\gamma$ -camera imaging of  $^{99\text{m}}\text{Tc}$  provided a noninvasive method to track the behavior of Tc at ultra-trace ( $< 10^{-10}$  mol l $^{-1}$ ) concentrations alongside the related reactivity of Fe(II) and extant microbial ecology. Columns were established under a flow regime representative of proposed biostimulation at the Sellafield nuclear facility and, for the first time, were tested for  $^{99\text{m}}\text{Tc(VII)}$  reactivity across a range of biogeochemical conditions.

## Methods

### Sediment

Sediments representative of the Quaternary unconsolidated alluvial flood-plain deposits that underlie the UK Sellafield reprocessing site were collected from the Calder Valley, Cumbria, from a well characterised field site (Law et al. 2010; Thorpe et al. 2012). Sediments were transferred directly into sterile containers, sealed, and stored at 4 °C prior to use.

### Column design and setup

Four Perspex columns (20 cm  $\times$  4 cm i.d.), total volume 250 cm $^3$ , were each packed with  $\sim 225$  g (volume 210 cm $^3$ ) of moist sediment. The base of each column consisted of a  $\sim 1$  cm plug of glass fiber wool and  $\sim 1$  cm quartz sand, and at the top a  $\sim 1$  cm plug of glass fiber wool terminated the column. An array of columns using synthetic regional groundwater (Wilkins et al. 2007) amended with 1 mM nitrate was set up with an upflow configuration, and a flow rate of 4.3 ml hr $^{-1}$  (using a Watson–Marlow peristaltic pump) with experiments maintained at room temperature in the dark.

The pH of influent groundwater was 6.9–7.1 throughout the experiment and it was pumped into each column from separate, sterile reservoirs, which were changed every 6 days. In these experiments, the temporal variations in biostimulation and biomineralization were explored. The effective pore volume, expressed as a percentage of the total volume of the columns at the start of the experiment, was determined by the addition of  $6 \times 10^{-5}$  M Br $^-$  as a conservative tracer and analysis of the Br $^-$  breakthrough curve.

### Sampling and geochemical analysis

The column influent and effluent were monitored periodically with pH, Eh, and concentrations of acetate,  $\text{SO}_4^{2-}$ ,  $\text{NO}_2^-$ ,  $\text{NO}_3^-$ , Fe(II), Fe, Mn, Al, Si and Mg used to track the progress of sediment bioreduction. Key geochemical indicators such as the appearance of  $\text{NO}_2^-$ ,  $\text{Mn}_{(\text{aq})}$  and  $\text{Fe}_{(\text{aq})}$ , Fe(II), and the disappearance of  $\text{SO}_4^{2-}$  and  $\text{NO}_3^-$  in the effluent were used to track the progress of terminal electron accepting processes and the onset of nitrate, manganese, iron and sulfate reduction. Porewater  $\text{NO}_2^-$  Mn and Fe(II) were measured by spectrophotometric methods (Goto et al. 1997; Harris and Mortimer 2002; Lovley and Philips 1987; Viollier et al. 2000).

Groundwater cation concentrations (Mg, Al, Fe, Mn, Sr and Ca) were measured by ICP-AES with good agreement between Fe(II) and Mn measured by spectroscopic methods. Acetate,  $\text{SO}_4^{2-}$ ,  $\text{NO}_2^-$ ,  $\text{NO}_3^-$  were measured by ion chromatography. Aqueous manganese concentrations are reported as total  $\text{Mn}_{(\text{aq})}$  and under these experimental conditions  $\text{Mn}_{(\text{aq})}$  is expected to be speciated as Mn(II). Similarly  $\text{Fe}_{(\text{aq})}$  values are reported as  $\text{Fe}(\text{total})_{(\text{aq})}$  as measured by ICP-AES. Simultaneous ferrozine measurements on a subset of samples confirmed that  $> 95\%$  of  $\text{Fe}_{(\text{aq})}$  was present as Fe(II) and thus  $\text{Fe}(\text{total})_{(\text{aq})}$  data were dominated by  $\text{Fe}(\text{II})_{(\text{aq})}$ . Eh and pH were measured using calibrated electrodes (Denver-Basic).

Following  $^{99m}\text{Tc}$  imaging, columns were allowed to radiologically decay (at  $4^\circ\text{C}$  for 5 days) and then sampled at 2 cm intervals along the core to allow measurement of solid phase 0.5 N HCl extractable Fe(II) and  $\text{Fe}_{\text{total}}$  as a proxy for Fe(III)-reduction. Here, sediments were digested in 0.5 N HCl for 1 h followed by ferrozine analysis. The first sample from each column was taken at 2 cm at the interface between the quartz sand and the sediment. Sediment chemical composition was measured by X-ray fluorescence (Thermo ARL 9400 XRF) and total organic and inorganic carbon was measured using a Shimadzu TOC-L analyzer.

### Gamma camera imaging and analysis

Column experiments were prepared with variable incubation times so that each column was at a different stage of bioreduction (targeting oxic, early metal-reducing, Fe(III)-reducing and sulfate-reducing conditions) at the point at which the  $\gamma$ -camera imaging occurred. At this point, columns were transported to the Nuclear Medicine Center at the Manchester Royal Infirmary, where  $^{99m}\text{Tc}(\text{VII})\text{O}_4^-$  was introduced to the base of each column as a 1-ml spike of  $\sim 9.61$  MBq  $^{99m}\text{Tc}$  ( $5 \times 10^{-10}$  mol  $\text{l}^{-1}$ ). Technetium-99m is a metastable nuclear isomer of  $^{99}\text{Tc}$  with a short half-life (6 h) and decays to  $^{99}\text{Tc}$  by gamma emission (140 keV). Imaging of the gamma rays emitted from the columns took place with a Siemens Symbia T6 dual-headed gamma camera (2 mm holes, estimated  $\pm 2$  mm accuracy). The flow rate of  $4.3$  ml  $\text{h}^{-1}$  allowed for  $\sim 1.4$  column pore volumes to pass through each column over the 12 hour experiment and representing an approximate dilution factor for the spike of  $70\times$  over the 12-h period (from  $5 \times 10^{-10}$  mol  $\text{l}^{-1}$  to a final concentration in the order of  $7 \times 10^{-12}$  mol  $\text{l}^{-1}$  assuming ideal dilution). After injection,  $\gamma$ -camera images of all four column experiments were taken at 20 min intervals with a total of 36 images per column collected.

Data analysis for  $^{99m}\text{Tc}$  activities and images from  $\gamma$ -camera data acquisition were conducted using GE Xeleris medical imaging software (GE Medical Systems, USA). Data for  $^{99m}\text{Tc}$  at time points taken at 20-min intervals were background subtracted and decay corrected to the initial timeframe. Errors reported on  $^{99m}\text{Tc}$  activities refer to  $\gamma$ -camera counting accuracy as repeat analyses were not possible.

## Results and discussion

### Column geochemistry

The microbially available Fe(III)-content of the sediment prior to bioreduction, as estimated by a 1 h 0.5 N HCl digestion on 5 replicates of 0.1 g of sediment, was  $7.2 \pm 0.5$  mmol  $\text{Kg}^{-1}$ . The

total iron content of the sediment was  $3.2 \pm 0.1$  wt% Fe ( $57$   $\mu\text{mol g}^{-1}$ ) and therefore  $12.6 \pm 0.9\%$  of the Fe(III) was “bioavailable” at the start of the experiment. Total organic carbon in the sediment was  $0.44 \pm 0.04\%$ .

In four columns, saturated flow was established for 5, 21, 35 and 100 days such that on the day of  $\gamma$ -camera imaging the columns represented “oxic,” “early metal-reducing,” “Fe(III)-reducing” and “sulfate-reducing” conditions, respectively. In the oxic control column, acetate was not added to influent groundwater and no changes occurred in effluent nitrate, Fe or sulfate over the 5 days of saturated flow prior to  $\gamma$ -camera imaging and the effluent pH was 5.2.

In the early metal-reducing column nitrate, present at 1 mM in the influent groundwater, and nitrite, a by-product of nitrate reduction, were depleted in the effluent within 7 days indicating that a robust nitrate-reducing community was present and that denitrification was occurring (data not shown). The pH of the effluent also increased over the 21 days from 5.2 to 6.4 and this was attributed to the ongoing denitrification and subsequent release of  $\text{OH}^-$  and  $\text{HCO}_3^-$  into solution (Law et al. 2010; Thorpe et al. 2012). At 21 days  $\text{Mn}_{(\text{aq})}$  ( $17$   $\mu\text{M}$ ) and minor  $\text{Fe}_{(\text{aq})}$  ( $23$   $\mu\text{M}$ ) were detected in the effluent indicating the establishment of early metal-reducing conditions (Table 1; Figure 1). The appearance of Fe in effluent water most likely occurred a few days after the onset of Fe(III) reduction which is often observed in sediment Fe(II)/Fe<sub>total</sub> ratios prior to ingrowth of  $\text{Fe(II)}_{\text{aq}}$  to porewaters (Burke et al. 2005; Islam et al. 2004)."

In the Fe(III)-reducing column, nitrate was depleted within 7 days and the pH increased over 35 days from 5.1 to 7.2, again presumably due to ongoing reduction of the influent nitrate. Following nitrate depletion, aqueous Mn and Fe were also detected in the column effluent, increasing to 1.25 mM and 0.23 mM respectively after 35 days (Table 1; Figure 1).

In the sulfate-reducing column terminal electron accepting processes proceeded at a similar rate to the early metal-reducing, and Fe(III)-reducing columns and the pH stabilized at 7.2 during the 100-day incubation. Here, total aqueous Fe in the effluent was at a maximum of 0.25 mM between 35 and 40 days and decreased to  $<10$   $\mu\text{M}$  by 100 days. A fall in the concentration of aqueous Fe in the effluents did not signify the end of Fe(III) reduction, but rather that Fe was likely being retained within the column. This was presumably due to the increased pH causing Fe(II) to sorb more strongly to mineral surfaces and promoting the formation of Fe(II)-bearing mineral phases as they became oversaturated. In addition, from 25 days, sulfate in the effluent decreased compared to influent concentrations and by 100 days, no sulfate was observed in the effluent suggesting active sulfate reduction was occurring. There was visual evidence for the formation of iron sulfides

**Table 1.** Geochemistry of the columns on the day of  $^{99m}\text{Tc}(\text{VII})\text{O}_4^-$  addition and gamma camera imaging.

Column conditions	Days of flow	pH	$\text{Mn}_{(\text{aq})}$ (mM)	$\text{Fe}_{(\text{aq})}$ (mM)	Sulfate (mM)
Oxic	5	$5.5 \pm 0.1$	$0.00 \pm 0.001$	$0.00 \pm 0.001$	$0.44 \pm 0.004$
Early metal reducing	21	$6.4 \pm 0.1$	$0.17 \pm 0.002$	$0.02 \pm 0.002$	$0.25 \pm 0.004$
Fe(III) reducing	35	$7.2 \pm 0.1$	$1.26 \pm 0.002$	$0.23 \pm 0.007$	$0.15 \pm 0.002$
Sulfate reducing	100	$7.2 \pm 0.1$	$0.02 \pm 0.003$	$0.01 \pm 0.002$	$0.01 \pm 0.001$

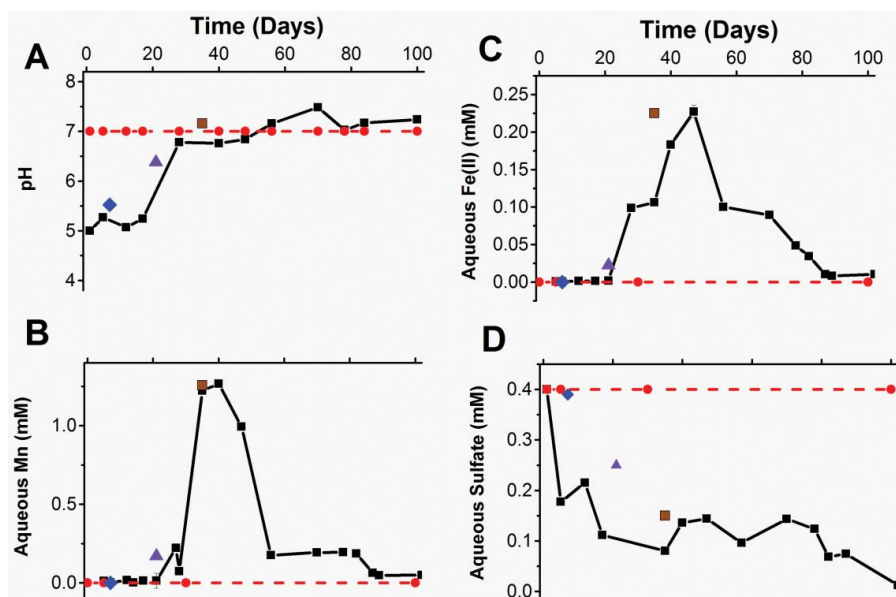


**Figure 1.** Geochemistry of the longest running, sulfate-reducing, column and end point geochemistry for the oxic, early metal-reducing and Fe(III)-reducing columns. A) pH, B) aqueous Fe(II), C) aqueous Mn, D) sulfate in effluent porewaters from column experiments. Blue diamonds = oxic column at time of  $^{99m}\text{Tc}$  imaging, purple triangles = early metal reducing column at the time of imaging, brown squares = Fe(III) reducing column at the time of imaging, and black squares = sulfate reducing column over the 100 days under flow conditions.

and olfactory evidence for the production of Sulfide. Geochemical modelling of the column porewater in PHREEQC-2 (Minneteq.v4 database) using the measured effluent chemistry, aqueous Fe(II) estimated from the maximum concentration observed in porewaters, and pH of 7.2 predicted super-saturation with regard to FeS and mackinawite.

The various stages of bioreduction were identified using the column effluent geochemistry and the columns denoted as oxic, early metal-reducing, Fe(III)-reducing and sulfate-reducing, however post imaging dissection of the columns suggested heterogeneity as expected from such a dynamic system (Lear et al. 2010).

### $^{99m}\text{Tc}$ behavior in oxic sediment

The addition of a 1-ml spike of  $^{99m}\text{Tc}$  ( $\sim 9.6$  MBq;  $0.5 \times 10^{-10}$  mol  $\text{l}^{-1}$ ) to each column showed in varying  $^{99m}\text{Tc}$  retention on sediments over the 12-h period. In order to further quantify the distribution of the  $^{99m}\text{Tc}$  spike at the experimental end point, the  $^{99m}\text{Tc}$  image from each column was divided into four equal 5-cm segments (0–5 cm, 5–10 cm, 10–15 cm and 15–20 cm). The retention of the spike in each segment was then calculated as the percentage of the original injected activity.

After decay storage, the column was destructively sampled at 2-cm intervals and analyzed for 0.5 N HCl extractable Fe(II)/Fe(III). In the oxic column, there was no evidence for Fe(II) ingrowth to sediments and the experimental end point confirmed that  $^{99m}\text{Tc}$  did not associate significantly with column sediments (Table 1; Figures 2 and 3). This was unsurprising as  $^{99m}\text{Tc}$  imaging has shown essentially conservative behavior of Tc(VII) under oxic conditions (Burke et al. 2010; Corkhill et al. 2013; Vandahey et al. 2012). At the final experimental time point, <5% of the  $^{99m}\text{Tc}$  spike remained in the lower quarter of the column possibly due to retention in unconnected pore spaces or weak sorption of  $\text{TcO}_4^-$  to positively charged mineral

surfaces at the low pH of the system (pH 5.5) (Peretyazhko et al. 2012).

Interestingly, the  $^{99m}\text{Tc}$  imaging in the oxic core showed brighter intensity in the center of the column suggesting that a preferential flow path had developed (Figure 2). This was supported by analysis of the column breakthrough point at  $t = 0$  (with  $\text{Br}^-$ ) at 10.9 h and at  $t = 5$  days (with  $^{99m}\text{Tc}$ ) at 6.8 h. This translated to a significant reduction in the effective porosity of the column during the experimental run (from 22% porosity to 14% porosity) presumably due to settling and / or flow path evolution. The groundwater transport rate at the time of imaging was therefore in the order of  $4 \times 10^{-6}$  m  $\text{s}^{-1}$ , which is in the range of flow rates reported at the Sellafield and Hanford sites ( $3\text{--}7 \times 10^{-6}$  m  $\text{s}^{-1}$ ; Marshall et al. 2014; Waichler and Yabusaki 2005).

### $^{99m}\text{Tc}$ behavior following bioreduction

Prior to imaging, the pH of the early metal- (21 days), Fe(III)- (35 days), and sulfate (100 days)-reducing columns was 6.4, 7.2 and 7.2, respectively. Gamma camera images over the 12 h following spiking with  $^{99m}\text{Tc}(\text{VII})\text{O}_4^-$  showed significant (> 98%) retention of  $^{99m}\text{Tc}$  in all of the bioreducing columns. Interestingly, there were differences in the rate of  $^{99m}\text{Tc}$  reaction and consequent flow under the varying biogeochemical conditions (Figure 2). The rate of  $^{99m}\text{Tc}$  sequestration to sediments increased with decreasing redox potential and increasing pH, presumably reflecting an increase in both sediment associated and biomineral Fe(II) which is more reactive toward technetium(VII) than aqueous Fe(II) (Lee et al. 2014; Lloyd et al. 2000; Peretyazhko et al. 2012; Zachara et al. 2007).

In the early metal-reducing column, the percentage of 0.5 N extractable Fe present as Fe(II) measured 1–2% at 2 cm and 4 cm ( $\sim 0.1$   $\mu\text{mol s g}^{-1}$ ), increased significantly to 14% by 6 cm, and averaged  $15 \pm 4\%$  ( $\sim 1.4$   $\mu\text{mol s g}^{-1}$ ) thereafter to the top

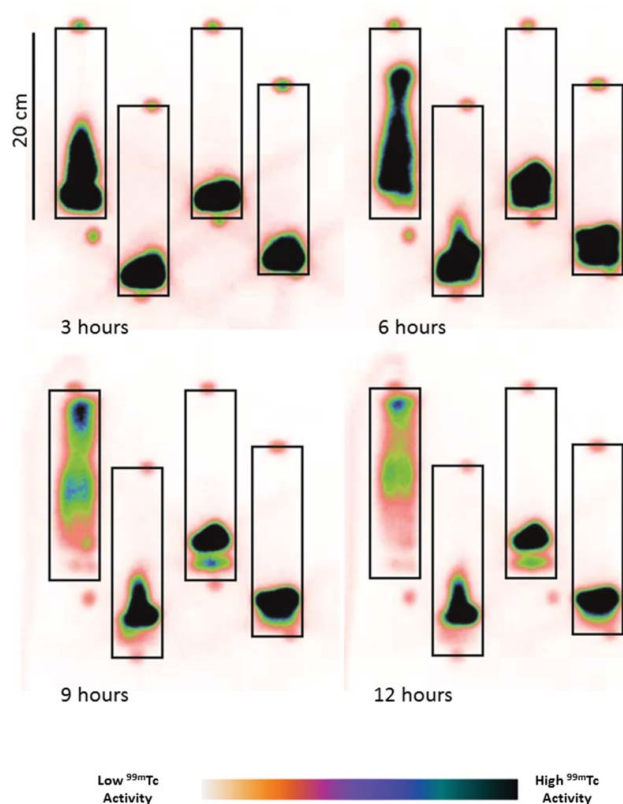


**Figure 2.** Color-inverted image of Tc-99 transport through columns after 3, 6, 9 and 12 hours incubation in, from left to right, oxic, early metal reducing, Fe(III) reducing and sulfate reducing columns.

of the column (Figure 3). Quantitative analysis of the spike distribution at the 12-h end-point showed 69% of the spike was retained in the first 5 cm of the column with 28% of the spike in the 5–10 cm fraction, 1.3% in the 10–15 cm fraction and 0.9% in the 15–20 cm section (Figures 3 and 4).

Interestingly, these results show that  $^{99m}\text{Tc}$  was moving within the sediment core even though Fe(II) in the 0–5 cm segment of the core was between  $0.1\text{--}1\ \mu\text{mol g}^{-1}$  at least a  $10^5\text{--}10^6$  times excess compared to the  $^{99m}\text{Tc}$  spike. As Fe(II) is present in significant excess, this result therefore implies that  $^{99m}\text{Tc}$

mobility is related to its reduction rate which in turn is linked to Fe(II) speciation in the columns (Burke et al. 2010; Peretyazhko et al. 2012; Zachara et al. 2007). The pH of the early metal reducing column was 6.4 and was therefore lower than the pH in the Fe(III)- and sulfate-reducing columns at 7.2.

The lower pH value means that a higher proportion of the Fe(II) produced from microbial reduction is likely to be present as  $\text{Fe(II)}_{(\text{aq})}$ , which is less effective as a fast reductant for Tc(VII) than sorbed or mineral bound Fe(II). Thus we postulate that the Fe(II) speciation in the early metal reducing column resulted in slow rates of Tc(VII) reduction compared to sorbed and mineral associated Fe(II) (Fredrickson et al. 2004; Lloyd et al. 2000; Peretyazhko et al. 2012; Zachara et al. 2007). Enhanced Tc(VII) mobility in this column may therefore be attributed to a lower pH impacting the speciation of the biogenic Fe(II) with more Fe(II) aqueous and less sorbed and mineral associated Fe(II) and thus a slower rate of  $^{99m}\text{Tc}$  reduction.

In the Fe(III)-reducing column the percentage of 0.5 N HCl extractable Fe as Fe(II) measured 21 and 24% at 2 cm and 4 cm, respectively ( $\sim 1.6\ \mu\text{mols g}^{-1}$ ), increasing to 58% at 6 cm and then averaged  $51 \pm 4\%$  ( $\sim 3.6\ \mu\text{mols g}^{-1}$ ) in the rest of the column (Figure 3). This meant in the first 0–5 cm of the column there was  $1.6\ \mu\text{mols g}^{-1}$  Fe(II) in sediments. Quantitative analysis of the spike distribution at the 12-h end-point showed 87% of the spike was retained in the first 5 cm of the column with 13% of the spike in the 5–10 cm fraction and less than 0.5% in the 10–15-cm and 15–20-cm sections (Figure 4). These results indicate faster Tc(VII) reduction rates in this column than in the early metal reducing column. We attribute this to the increased pH of 7.2 observed in the column effluent and the likely resulting increase in sediment / mineral bound Fe(II) which has been shown to be more reactive towards Tc(VII) than aqueous Fe(II) (Peretyazhko et al. 2012; Zachara et al. 2007).

In the sulfate-reducing column Fe(III) reduction was well established and 0.5% N extractable Fe as Fe(II) measured 72% at 2 cm and averaged  $79.8 \pm 6.3\%$  thereafter, making the concentration of sediment associated Fe(II)  $\sim 4.8\ \mu\text{mols g}^{-1}$  in the 0–5 cm column segment and  $\sim 5.2\ \mu\text{mols g}^{-1}$  thereafter

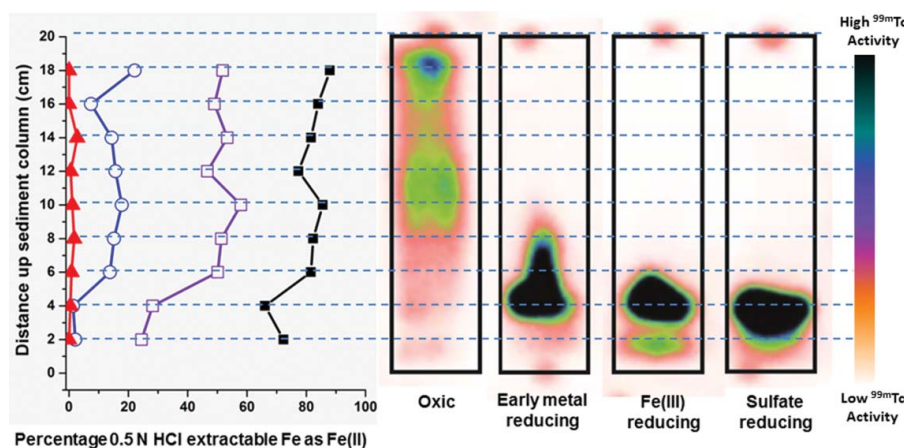


**Figure 3.** (Left) percentage of 0.5 N extractable Fe(II)/Fe(III) present at 2 cm intervals up the sediment column, and (Right) activity of  $^{99m}\text{Tc}$  accumulated in each 2 cm interval for black) oxic column, red) early metal reducing column, blue) Fe(III)-reducing column and purple) sulfate-reducing column. Gamma emitting spot sources were used to mark the top of each column.

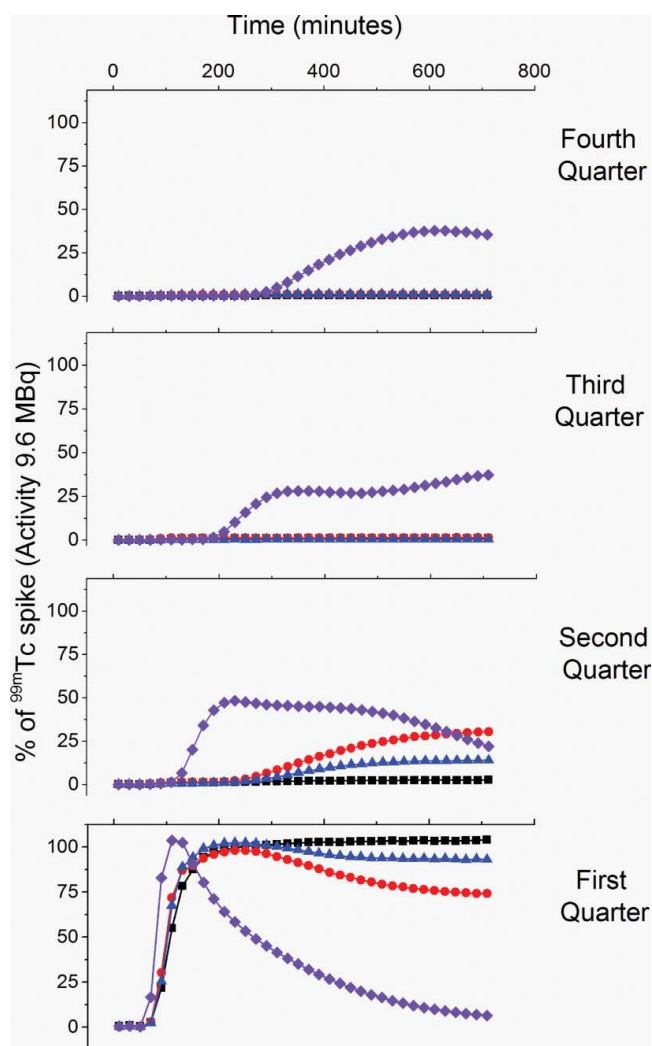


**Figure 4.** Activity of Tc in MBq in four quarters (first through fourth) along the flow direction of each column where black = sulfate reducing, red = Fe(III) reducing, blue = early metal reducing, and purple = oxic conditions.

(Figure 3). Here 96% of the  $^{99m}\text{Tc}$  spike was retained at 0–5 cm, with only 3% of the  $^{99m}\text{Tc}$  detected from 5–10 cm and  $^{99m}\text{Tc}$  below background in the 10–15 and 15–20-cm fractions (Figure 4).

Here, the  $^{99m}\text{Tc}$  sequestration to solids appeared faster than under Fe(III) reducing conditions despite identical pH and similar Fe(II) concentrations in sediments (Fe(III)-reducing =  $\sim 2.4 \mu\text{mols g}^{-1}$ ; sulfate-reducing =  $4.8 \mu\text{mols g}^{-1}$ ). We therefore attribute this to the presence of Fe(II) sulfide biominerals such as mackinawite, a poorly structured precursor to pyrite, or amorphous iron sulfides. Iron sulfide bearing sediments show reduction rates for Tc in the order of a few minutes (and relevant to reaction over the 20-min exposure times for gamma camera imaging used here) and have the highest reported  $K_d$  values for  $^{99}\text{Tc}$  in the literature (Burke et al. 2010).

### Implications

These experiments are the first to image ultra-trace  $^{99m}\text{Tc}$  transport in a set of dynamic columns representing variable

biogeochemistry associated with biostimulation of nuclear site sediments. Results demonstrate an increase in the rate of Tc (VII) reductive sequestration in progressively more reducing columns, with sediment pH playing an important role in regulating the amount of sorbed / biomineral associated Fe(II) available to react with Tc(VII). Further, progression of terminal electron accepting processes through to sulfate reduction appears to lead to the fastest rates of  $^{99m}\text{Tc}$  sequestration presumably due to the presence of sulfide phases.

These results highlight the importance of both groundwater pH and Fe(II) speciation in controlling Tc(VII) reduction rates. Furthermore, results show that in these gamma camera imaging is a useful tool both to investigate the flow regimes within sediment columns and to image reactive Fe(II) in sediments, but that it needs to be carefully coupled to biogeochemical measurements to fully interpret Tc reactions in complex systems. Overall, our results present a positive outlook for the use of bioreduction in technetium contaminated environments and extends previous work showing Tc(VII) is removed from solution concurrent with Fe(III)-and sulfate-reducing conditions to ultra-dilute concentrations of  $^{99m}\text{Tc}$ . Sulfate reducing conditions at ambient pH resulted in the most rapid removal of  $^{99m}\text{Tc}$  at  $\sim 10\text{--}12 \text{ mol l}^{-1}$  concentrations to sediment.

### Acknowledgments

We thank Alastair Bewsher and Paul Lythgoe for help in data acquisition. We thank Julian Cruickshank and the Sellafield Land Quality team for their collaboration and input.

### Funding

This work was supported University of Manchester EPSRC Impact Acceleration Account and Sellafield Ltd. We also acknowledge the support of the Natural Environment Research Council (Grant NE/H007768/1).

### References

- Beals DM, Hayes DW. 1995. Technetium-99, iodine-129 and tritium in the waters of the Savannah River Site. *Sci Total Environ* 1:173–174.
- Bishop ME, Dong H, Kukkadapu RK, Liu C, Edelmann RE. 2012. Bioreduction of Fe-bearing clay minerals and their reactivity toward pertechnetate (Tc-99). *Geochim Cosmochim Acta* 75(18):5229–5246.
- Burke IT, Boothman C, Lloyd JR, Mortimer RJM, Livens FR, Morris K. 2005. Effects of progressive anoxia on the solubility of technetium in sediments. *Environ Sci Technol* 39:4109–4116.
- Burke IT, Livens FR, Lloyd JR, Brown AP, Law GTW, McBeth JM, Ellis BL, Lawson RS, Morris K. 2010. The fate of technetium in reduced estuarine sediments: combining direct and indirect analyses. *Appl Geochem* 25:233–241.
- Corkhill CL, Bridge JW, Chen XC, Hillel P, Thornton SF, Romero-Gonzalez ME, Banwart SA, Hyatt NC. 2013. Real-time gamma imaging of technetium transport through natural and engineered porous materials for radioactive waste disposal. *Environ Sci Technol* 47:13857–13864.
- Eagling J, Worsfold PJ, Blake WH, Keith-Roach MJ. 2012. Mobilization of technetium from reduced sediments under seawater inundation and intrusion scenarios. *Environ Sci Technol* 46:798–803.
- Fredrickson JL, Zachara JM, Kennedy DW, Kukkadapu RK, Mckinley JP, Heald SM, Liu C, Plymale AE. 2004. Reduction of  $\text{TcO}_4^-$  by sediment-associated biogenic Fe(II). *Geochim Cosmochim Acta* 68:3171–3187.
- Goto K, Taguchi S, Fukue Y, Ohta K, Watanabe H. 1997. Spectrophotometric determination of manganese with 1-(2-pyridylazo)-2-naphthol and a non-ionic surfactant. *Talanta* 24:752–753.

- Harris SJ, Mortimer RJG. 2002. Determination of nitrate in small water samples by the cadmium-copper reduction method: A manual technique with application to the interstitial waters of marine sediments. *Inter J Environ Anal Chem* 82:369–376.
- Hess NJ, Xia YX, Rai D, Conradson SD. 2004. Thermodynamic model for the solubility of  $\text{TcO}_2 \cdot x\text{H}_2\text{O}(\text{am})$  in the aqueous  $\text{Tc}(\text{IV})\text{-Na}^+\text{-Cl}^-\text{-H}^+\text{-OH}^-\text{-H}_2\text{O}$  system. *J. Sol. Chem.* 33:199–226.
- Icenhower JP, Oafoku NP, Zachara JM, Martin WJ. 2010. The biogeochemistry of technetium: A review of the behavior of an artificial element in the natural environment. *Amer J Sci* 310:721–752.
- Islam FS, Gault AG, Boothman C, Polya DA, Charnock JM, Chatterjee D, Lloyd JR. 2004. Role of metal-reducing bacteria in arsenic release from Bengal delta sediments. *Nature*, 430, 68–71.
- Law GTW, Geissler A, Boothman C, Burke IT, Livens FR, Lloyd JR, Morris K. 2010. Role of nitrate in conditioning aquifer sediments for technetium bioreduction. *Environ Sci Technol* 44:150–155.
- Lear G, McBeth JM, Boothman C, Gunning DJ, Ellis BL, Lawson RS, Morris K, Burke IT, Bryan ND, Brown AP, Livens FR, Lloyd JR. 2010. Probing the biogeochemical behavior of technetium using a novel nuclear imaging approach. *Environ Sci Technol* 44:156–162.
- Lee J, Zachara JM, Fredrickson JK, Heald SM, McKinley JP, Plymale AE, Resch CT, Moore, DA. 2014. Fe(II)- and sulfide-facilitated reduction of  $^{99}\text{Tc}(\text{VII})\text{O}_4^-$  in microbially reduced hyporheic zone sediments. *Geochim Cosmochim Acta* 136:247–264.
- Liu C, Gorby YA, Zachara JM, Fredrickson JK, Brown CF. 2002. Reduction kinetics of Fe(III), Co(III), U(VI), Cr(VI), and Tc(VII) in cultures of dissimilatory metal-reducing bacteria. *Biotechnol Bioeng* 80(6):638–649.
- Liu Y, Terry J, Jurisson S. 2008. Pertechnetate immobilization with amorphous iron sulfide. *Radiochim Acta* 96:823–833.
- Liu J, Pearce CI, Qafoku OS, Arenholz A, Heald SM, Rosso KM. 2012. Tc(VII) reduction kinetics by titanomagnetite ( $\text{Fe}_3\text{-xTi}_x\text{O}_4$ ) nanoparticles. *Geochim Cosmochim Acta* 92:67–81.
- Livens FR, Jones MJ, Hynes AJ, Charnock JM, Mosselmann JFW, Hennig C, Steele H, Collison D, Vaughan DJ, Patrick RAD, Reed WA, Moyes LN. 2004. X-ray absorption spectroscopy studies of reactions of technetium, uranium and neptunium with mackinawite. *J Environ Radioact* 74:211–219.
- Lloyd JR, Sole VA, Van Praagh CVG, Lovley DR. 2000. Direct and Fe(II)-mediated reduction of technetium by Fe(II) reducing bacteria. *Appl Environ Microbiol* 66:3743–3749.
- Lovley DR, Phillips EJP. 1987. Rapid assay for microbially reducible ferric iron in aquatic sediments. *Appl Environ Microbiol* 53:1536–1540.
- McBeth JM, Lloyd JR, Law GTW, Livens FR, Burke IT, Morris K. 2011. Redox interactions of technetium with iron-bearing minerals. *Mineral Mag* 75(4):2419–2430.
- Marshall A, Coughlin D, Laws, F. 2014. Groundwater monitoring at Sellafield, annual data review 2014. Sellafield Ltd. Report No: LQTD00080.
- Marshall MJ, Plymale AE, Kennedy DW, Shi L, Wang Z, Reed SB, Dohnalkova AC, Simonson CJ, Liu C, Saffarini DA, Romine MF, Zachara JM, Beliaev AS, Fredrickson JK. 2008. Hydrogenase- and outer membrane c-type cytochrome-facilitated reduction of technetium(VII) by *Shewanella oneidensis* MR-1. *Environ Microbiol* 10(1):125–136.
- Morris K, Livens FR, Charnock JM, Burke IT, McBeth JM, Begg JDC, Boothman C, Lloyd JM. 2008. An X-ray absorption study of the fate of technetium in reduced and reoxidised sediments and mineral phases. *Appl Geochem* 23:603–617.
- Newsome L, Morris K, Lloyd JR. 2014. The biogeochemistry and bioremediation of uranium and other priority radionuclides. *Chem Geol* 363:164–184.
- Pepper SE, Bunker DJ, Bryan ND, Livens FR, Charnock JM, Patrick RAD, Collison D. 2003. Treatment of radioactive wastes: An X-ray absorption spectroscopy study of the reaction of technetium with green rust. *J Coll Interf Sci* 268:408.
- Peretyazhko TS, Zachara JM, Kukkadapu RK, Heald SM, Kutnyakov IV, Resch CT, Arey BW, Wang CM, Kovarik L, Phillips JL, Moore DA. 2012. Pertechnetate ( $\text{TcO}_4^-$ ) reduction by reactive ferrous iron forms in naturally anoxic, redox transition zone sediments from the Hanford Site, USA. *Geochim Cosmochim Acta* 92:48–66.
- Plymale AE, Fredrickson JK, Zachara JM, Dohnalkova AC, Heald SM, Moore DA, Marshall MJ, Wang CM, Resch CT, Nachimuthu P. 2011. Competitive reduction of pertechnetate ( $^{99}\text{TcO}_4^-$ ) by dissimilatory metal reducing bacteria and biogenic Fe(II). *Environ Sci Technol* 45:951–957.
- Prakash D, Gabani P, Chandel AK, Ronen Z, Singh OV. 2013. Bioremediation: a genuine technology to remediate radionuclides from the environment. *Microb Biotechnol* 6(4): 349–360.
- Serne RJ, Rapko BM. 2014. Technetium inventory, distribution and speciation in Hanford tanks, U.S. Department of Energy Report, PNNL-23319, EMSP-RPT-022. Available at: [http://www.pnnl.gov/main/publications/external/technical\\_reports/PNNL-23319.pdf](http://www.pnnl.gov/main/publications/external/technical_reports/PNNL-23319.pdf)
- Thorpe CL, Law GTW, Boothman C, Lloyd JR, Burke IT, Morris K. 2012. Synergistic effect of high nitrate concentrations on sediment bioreduction. *Geomicrobiol J* 29:484–493.
- Thorpe CL, Boothman C, Lloyd JR, Law GTW, Bryan ND, Atherton N, Livens FR, Morris K. 2014. The interactions of strontium and technetium with Fe(II) bearing biominerals: Implications for bioremediation of radioactively contaminated land. *Appl Geochem* 40:135–143.
- Vandehey NT, O'Neil JP, Slowey AJ, Boutchko R, Druhan JL, Moses WW, Nico PS. 2012. Monitoring Tc dynamics in a bioreduced sediment: an investigation with gamma camera imaging of ( $^{99m}\text{Tc}$ ) Tc-pertechnetate and ( $^{99m}\text{Tc}$ ) Tc-DTPA. *Environ Sci Technol* 46:12583–12590.
- Viollier E, Inglett PW, Hunter K, Roychoudhury AN, Van Cappellen P. 2000. The ferrozine method revisited: Fe(II)/Fe(III) determination in natural waters. *Appl Geochem* 15:785–790.
- Waichler SR, Yabusaki SB. 2005. Flow and Transport in the Hanford 300 Area Vadose Zone-Aquifer-River System, Pacific National Nuclear Laboratory report-15125. Available at: [http://www.pnl.gov/main/publications/external/technical\\_reports/PNNL-15125.pdf](http://www.pnl.gov/main/publications/external/technical_reports/PNNL-15125.pdf)
- Wildung RE, Li SW, Murray CJ, Krupka KM, Xie Y, Hess NJ, Roden EE. 2004. Technetium reduction in sediments of a shallow aquifer exhibiting dissimilatory iron reduction potential. *FEMS Microbiol Ecol* 49:151–162.
- Wilkins MJ, Livens FR, Vaughan DJ, Beadle I, Lloyd JR. 2007. The influence of microbial redox cycling on radionuclide mobility in the subsurface at a low-level radioactive waste storage site. *Geobiology* 5:293–301.
- Zachara RT, Heald SM, Jeon B-H, Kukkadapu RA, Liu C, McKinley JP, Dohnalkova AC, Moore DA. 2007. Reduction of pertechnetate ( $\text{Tc}(\text{VII})$ ) by aqueous Fe(II) and the nature of the solid phase redox products. *Geochim Cosmochim Acta* 71:2137–2157.